

Epitope Fine Mapping by Mass Spectrometry: Investigations of Immune Complexes Consisting of Monoclonal Anti-HpTGEKP Antibody and Zinc Finger Protein Linker Phospho-Hexapeptides

Maximilian Scherf,^[a] Bright D. Danquah,^[a] Cornelia Koy,^[a] Peter Lorenz,^[b] Felix Steinbeck,^[b, c] Andrei Neamtu,^[d] Hans-Jürgen Thiesen,^[b, c] and Michael O. Glocker^{*[a]}

Accurate formation of antibody-antigen complexes has been relied on in both, multitudes of scientific projects and ample therapeutic and diagnostic applications. Mass spectrometrically determined dissociation behavior of immune complexes with the anti-HpTGEKP antibody revealed that the ten most frequently occurring phospho-hexapeptide linker sequences from C2H2 zinc finger proteins could be divided into two classes: orthodox binders, where strong noncovalent interactions developed as anticipated, and unorthodox binders with deviating structures and weaker binding. Phosphorylation of

threonine was compulsory for antibody binding in an orthodox manner. Gas phase dissociation energy determinations of seven C2H2 zinc finger protein linker phospho-hexapeptides with orthodox binding properties revealed a bipolar binding motif of the antibody paratope. Epitope peptides, which in addition to the negatively charged phospho-threonine residue were C-terminally flanked by positively charged residues provided stronger binding, *i.e.* dissociation was endothermic, than peptides with acidic amino acid residues at these positions, for which dissociation was exothermic.

Introduction

Zinc finger proteins comprise the largest class of transcription factors in man and the subclass of C2H2 zinc finger proteins are encoded by ca. 750 known genes.^[1] Zinc finger protein functions are extraordinarily diverse and include DNA recognition, RNA packaging, transcriptional activation, regulation of apoptosis, protein assembly, and lipid binding.^[2] Zinc finger proteins have been brought into context with human diseases including neurological disorders^[3] and because of their regulatory function on gene expression they are thought to play decisive roles in carcinogenic processes.^[4] On the other hand,

sequence-specific binding, a prerequisite for targeted gene expression regulation, predestines zinc finger proteins to be applied for genome editing and artificial modulation of gene expression.^[5] Zinc finger proteins possess a typical modular structure consisting of N-terminal protein interaction domains and C-terminally flanking arrays of several zinc finger domains through which binding to nucleobases is realized.^[6] There exist several thousand linker sequences with different amino acid sequences in human C2H2 zinc finger proteins; the HTGEKP motif being the one with highest occurrence.^[7] The linking amino acid sequences in between the zinc finger domain arrays of a zinc finger protein are known to fine-tune DNA-binding.^[8] Phosphorylation of the linkers' threonine (T) or serine (S) residue abolishes DNA binding of zinc finger proteins.^[9] Simultaneous phosphorylation of the majority of the cell's zinc finger proteins is considered a hallmark in the mitotic stage in eukaryotic cell replication^[10] whereas phosphorylation of particular zinc finger proteins has been found crucial for controlling processes of cellular differentiation and maturation.^[11]

The most prominent commercially available antibody which had been applied for elucidating cell biological regulatory networks with focus on zinc finger proteins had been raised against the HpTGEKP sequence motif^[9b] and has been applied to study the role of zinc finger proteins in cellular processes and for discovering some of the kinases which were to be made responsible for linker phosphorylation.^[12]

For specific binding of antibodies to their cognate antigens, defined forces must be exerted at specific interface locations. Yet, because the term "antibody specificity" is routinely used to declare that an antibody (solely) recognizes a certain (bio)molecule,^[13] terminology ought to be sharpened to better describe precise binding behavior on the sub-epitope level, *i.e.*

[a] M. Scherf, Dr. B. D. Danquah, Dr. C. Koy, Prof. Dr. M. O. Glocker
Proteome Center Rostock

University Medicine Rostock and University of Rostock
Schillingallee 69, 18059 Rostock (Germany)

E-mail: michael.glocker@uni-rostock.de

Homepage: <https://pzs.med.uni-rostock.de>

[b] Dr. P. Lorenz, F. Steinbeck, Prof. Dr. H.-J. Thiesen
Institute of Immunology

University Medicine Rostock

Schillingallee 70, 18059, Rostock (Germany)

[c] F. Steinbeck, Prof. Dr. H.-J. Thiesen
Gesellschaft für Individualisierte Medizin mbH (IndyMed)
Industriestrasse 15, 18069 Rostock (Germany)

[d] Prof. Dr. A. Neamtu
Department of Physiology
Gr. T. Popa University of Medicine and Pharmacy of Iasi
Str. Universitatii nr. 16, Iasi Jud. (Romania)

Supporting information for this article is available on the WWW under <https://doi.org/10.1002/cbic.202200390>

© 2022 The Authors. ChemBioChem published by Wiley-VCH GmbH. This is an open access article under the terms of the Creative Commons Attribution Non-Commercial License, which permits use, distribution and reproduction in any medium, provided the original work is properly cited and is not used for commercial purposes.

on the amino acid residue level which reveals either by nature or by design. Orthodox forces, *i.e.* noncovalent interactions according to generally accepted rules, between epitopes and paratopes unfold between single atoms placed on molecular partial surfaces with the right physicochemical properties on precisely matching positions on defined molecular surfaces located opposite to each other; see a more detailed discussion in reference [14]. With the terminology “orthodox/unorthodox” we describe binding mode differences on the sub-molecular level of one and the same antigen. One atom on an epitope surface may interact with more than one atom on a paratope surface and vice versa. The “sum of all atomic forces” required to strongly bind an epitope by the paratope is referred to by us the “molecular recognition code”. Pairing and force-exchange between amino acid residue atoms at the respective matching positions on the respective molecular surfaces of both, antigen and antibody, is the basis for the three-dimensional assembly of force-exchanging residues.

With our recently developed mass spectrometric method for determining epitope – paratope interactions, termed ITEM-TWO,^[15] a mass spectrometric method has become available which enables one to investigate epitope binding characteristics according to gas phase dissociation behavior of immune complexes. The acronym “ITEM-TWO” stands for “Intact Transition Epitope Mapping – Thermodynamic Weak-force Order”. In our previous work we have found that when comparing related epitope-antibody interactions with different binding strengths, the ranking of forces, *i.e.* the order of complex stabilities, is the same in the gas phase and in solution. Gas phase immune complex dissociation resembles in-solution characteristics of epitope – paratope interactions quite well.^[15a,b,16] Hence, ranking according to thermodynamic properties enables to qualitatively and quantitatively understand supramolecular binding specificities with direct access to decipher an antibody's recognition motif. Because of the zinc finger protein linkers' multitude, they provide an excellent naturally existing test system for investigating an epitope's key amino acid residues which constitute an antibody's “recognition code”.

In this work we interrogated which of the ten most abundant linker sequences from the human genome would be recognized as strong, weak, or non-binding sequence motifs of the monoclonal anti-HpTGEKP antibody. The ten most frequent zinc finger protein linker sequences, which represent 35% of all the linker sequences in man, were mixed, one by one, with the anti-HpTGEKP antibody in solution and binding properties were determined by analyzing gas phase dissociation energies of multiply charged immune complex ions. Based on our experimental data we distinguish orthodox antibody binding, exemplified by the phospho-hexapeptide HpTGEKP, from unorthodox immune complex formation, realized by non-canonical zinc finger protein linkers, such as HpTHTHT.

Results

Characterization of the monoclonal anti-HpTGEKP antibody and the synthetic epitope Peptides

The monoclonal anti-HpTGEKP antibody decorates phosphorylated zinc finger proteins from eukaryotic cell extracts which migrate by SDS-PAGE to the apparent mass range between approx. 60 kDa and 140 kDa as was found by Western blot analysis of protein extracts from HAP1 cell cultures (Figure 1A, lane 3). Okadaic acid, a phosphatase inhibitor, had been added to the cell cultures to preserve the *in-vivo* phosphorylation status of the zinc finger proteins during both, cell lysis and protein extract generation. Proteins were only faintly stained in the absence of phosphatase inhibitor in the cell culture medium, indicating that non-inhibited phosphatases had efficiently dephosphorylated the zinc finger proteins (Figure 1A, lane 2). Note, if an antibody binds its antigen in a Western blot, then there is a high chance that this antibody interacts with a sequential epitope and, hence, there remains a high chance that this antibody also interacts (in an orthodox fashion) with a peptide that encompasses the amino acid residues of the respective sequential epitope.

The nanoESI mass spectrum of the monoclonal anti-HpTGEKP antibody dissolved in ammonium acetate shows a symmetric charge state distribution of multiply protonated ion signals with Gaussian peak shapes (Figure 1B), proving a homogenous and contamination-free antibody preparation. Ion signals of the 23+ ion up to the 29+ ion were recorded and ion charge states and their *m/z* values (Supporting Information Table S1) calculate for an average molecular mass of 151,191 (\pm 47) Da.

Accordingly, the number of atoms for the anti-HpTGEKP phospho-hexapeptide antibody was estimated to be ca. 20,000, matching with the number of atoms from Rituximab, a monoclonal antibody with similar molecular mass and known amino acid sequence. Because of the hexapeptides' different amino acid compositions their calculated pI values vary

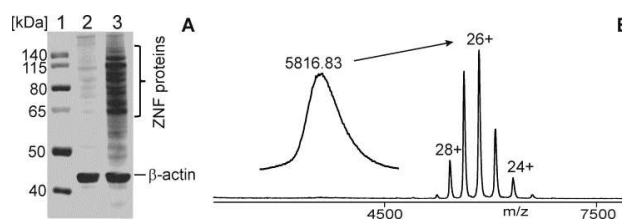


Figure 1. Structural and functional anti-HpTGEKP antibody characterization. (A) Western blot analysis of protein extracts from HAP1 (C631) cells. Lane 1: apparent molecular mass markers. Lane 2: Protein extract from cells without phosphatase inhibitor exposure. Lane 3: Protein extract from cells with exposure to okadaic acid. Proteins were subsequently decorated with the primary antibodies anti-HpTGEKP antibody and anti- β -actin antibody, respectively. IRDye 800 CW conjugated anti-mouse antibody from goat was used as secondary antibody. Blot images have been cropped above ca. 200 kDa and below ca. 35 kDa, respectively. (B) Nano-ESI mass spectrum of anti-HpTGEKP antibody. Charge states and *m/z* values for selected ion signals are given (*cf.* Supporting Information Table S1). The inset shows a zoom of the 26+ ion signal. Solvent: 200 mM ammonium acetate, pH 6.7.

between 4.29 and 9.67. Nano-ESI mass spectra of the ten synthetic phospho-hexapeptides (01–10) and of hexapeptide HTGEKP (00) dissolved in 200 mM ammonium acetate showed ion signals of singly and doubly protonated peptides with high purities and very little alkali salt adducts (Supporting Information Figures S1–S11). Neutral loss of phosphoric acid seemed typical for the phospho-hexapeptides' ions. The average number of atoms of each of the ten selected phospho-hexapeptides was ca. 100, as was determined from their elemental compositions (Table 1). Atom numbers of antibody, peptide and immune complex go into the ITEM-TWO calculations (see below). The unphosphorylated hexapeptide HTGEKP (00) served as control (*cf.* Table 1). Because mass spectra of all starting materials were well interpretable, both, the monoclonal anti-HpTGEKP antibody solution and the respective phospho-hexapeptide solutions with 200 mM ammonium acetate as solvents were found suitable for ITEM-TWO analyses.

Mass spectrometric binding strength analysis by ITEM-TWO

The ten phospho-hexapeptides (01–10), one by one, were mixed with monoclonal anti-HpTGEKP antibody in molar ratios of 3:1, each, for performing ITEM-TWO analyses. Thus, the mixtures consisting of excess peptides, free antibody, and immune complexes were electrosprayed to obtain desolvated ions. Ions were recorded upon mass spectrometric ion sorting without exclusion of any ions, *i.e.* upon transmission of all the ions to the instrument's detector. Mass spectra showed both, singly and doubly protonated peptide ion signals as well as multiply protonated anti-HpTGEKP antibody ion signals in addition to multiply protonated immune complex ion signals when immune complexes had formed as is illustrated with the phospho-hexapeptide HpTGERP (02)/anti-HpTGEKP antibody mixture (Supporting Information Figure S12A). Blocking transmission of low-mass ions using the quadrupole filtering

capabilities of the mass spectrometer prohibited recording of ion signals in the low-mass range (m/z 500– m/z 3900). Multiply charged ion signals in the high-mass range (m/z 3900– m/z 8000) were still detectable (Supporting Information Figure S12B).

The phospho-hexapeptide HpTGEKP (01)-anti-HpTGEKP antibody complex containing mixture showed the expected mixture of multiply charged antibody and immune complex ions as well (Figure 2A and Supporting Information Figure S13A). Peptide to antibody ratios of 1:1 and 2:1 are visualized by the satellite peaks on the high-mass sides of the multiply protonated antibody ion signals (Figure 2D). Dissociation of the immune complex ions was achieved by increasing the collision energy in the collision cell of the mass spectrometer and afforded singly charged ion signals of the previously bound peptides with isotopic resolution (Figure 2B). Because transmission of excess unbound peptide ions was blocked, the appearance of the singly protonated peptide ion signals proved binding and release of specifically bound phospho-hexapeptide HpTGEKP (01) from the immune complex (Figure 2B–2D and Supporting Information Figure S13B–S13D). The minor ion signal at m/z 748.34 (panel A, Figure 2) is explained by the excess of energy which is contained in a multiply charged and accelerated immune complex in the gas phase.

Table 1. Counts, isoelectric points, and numbers of atoms of zinc finger linker hexapeptides.

Linker peptide no.	Peptide sequence ^[a]	Count (frequency) ^[b]	pI ^[c,d]	Number of atoms ^[d]	Binding mode
00	HTGEKP	1692 (0.227)	7.59	92	n.a. ^[e]
01	HpTGEKP	1692 (0.227)	5.15	97	orthodox
02	HpTGERP	314 (0.042)	5.15	99	orthodox
03	HpSGEKP	217 (0.029)	5.15	94	unorthodox
04	HpTHTHT	65 (0.009)	6.30	101	unorthodox
05	HpTGKPP	58 (0.008)	9.67	102	orthodox
06	HpSGERP	56 (0.007)	5.15	96	orthodox
07	HpTGEKL	49 (0.006)	5.15	102	orthodox
08	HpTGEKS	48 (0.006)	5.15	94	unorthodox
09	HpTEEKP	45 (0.006)	4.29	106	orthodox
10	HpTREKP	43 (0.006)	7.59	113	orthodox

[a] Single letter code; small "p" indicates phosphorylation of following amino acid residue. [b] Total number of KRAB ZNF linker sequences (count) is 7465. Frequencies are rounded. [c] Calculated according to reference [17]. pK values for pS (5.60) and pT (5.90) are taken from reference [18]. [d] Calculated with GPMW version 10.30 (Lighthouse data, Odense, Denmark). [e] Not applicable.

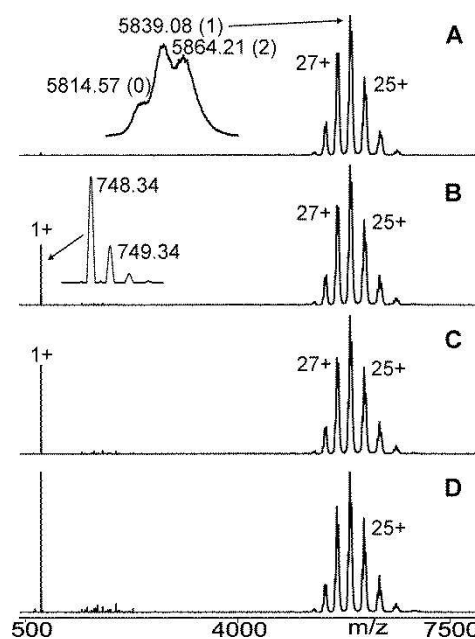


Figure 2. Nano-ESI mass spectra of the 1st measurement series of the phospho-hexapeptide HpTGEKP (01)-anti-HpTGEKP antibody immune complex dissociation analysis with increasing collision cell voltage differences (ΔCV): (A) 0 V, (B) 30 V, (C) 40 V, (D) 70 V. Charge states and m/z values for selected ion signals are given for the anti-HpTGEKP antibody and the immune complexes (antibody plus one peptide and antibody plus two peptides) on the right ion series. The inset in (A) shows a zoom of the 26+ ion signal. Numbers in parentheses indicate numbers of bound peptides. Complex-released singly-charged phospho-hexapeptide 01 ion signals are labelled on the left. The inset in (B) shows a zoom of the isotopically resolved peptide ion signals. For relative ion intensities refer to Supporting Information Tables S2 and S3. Solvent: 200 mM ammonium acetate, pH 6.7.

When collision energies were increased to very high values (collision cell voltage differences above 100 V), antibody fragment ions appeared in the middle mass range (m/z 2000– m/z 4000). In addition, peptide fragment ions which predominantly experienced neutral loss of phosphoric acid of the singly charged peptide ion appeared as well (Supporting Information Figure S14).

By contrast, absences of immune complex formations in peptide/antibody mixtures was instantly detected by either noting the lack of satellite ion signals of the multiply charged antibody ion signals in the high-mass range of the mass spectrum. Or by not observing complex-released peptide ion signals despite increasing collision energies in the low-mass range of the mass spectrum, as is illustrated with the hexapeptide HTGEKP (00)/anti-HpTGEKP antibody mixture (Supporting Information Figure S15).

Also of interest was the observation that in the phospho-hexapeptides/antibody mixtures which contained HpSGEKP (03; Supporting Information Figures S16 and S17), HpTHTHT (04, Supporting Information Figure S18), and HpTGEKS (08, Supporting Information Figures S19 and S20) there were no clear multiply charged satellite ion signals visible in the high-mass range. Instead, the multiply charged antibody ion signals were asymmetrically broadened on their high-mass sides. Most strikingly, singly or doubly charged ion signals of the peptides were seen only in low abundances in the low-mass ranges of the mass spectra despite blocking transmission of low-mass ions and increasing the collision energy. Presence of phospho-hexapeptide ions in the mass spectra indicated their origin as complex-released ion signals. However, the ion signal intensities did not increase proportionally with increasing collision energies, indicating peptide binding in an unorthodox manner (*cf.* Supporting Information Figure S21).

Opposite to the three binding peptides with unorthodox binding mode HpSGEKP (03), HpTHTHT (04), and HpTGEKS (08) the remaining seven phospho-hexapeptides HpTGEKP (01; Figure 2 and Supporting Information Figure S13), HpTGERP (02; Supporting Information Figure S22), HpTGKPP (05; Supporting Figures 23 and 24), HpSGERP (06; Supporting Figures 25 and 26), HpTGEKL (07; Supporting Information Figures S27 and S28), HpTEEKP (09; Supporting Information Figures S29 and S30), HpTREKP (10; Supporting Information Figures S31 and S32) bind in an orthodox manner as is judged by their immune complex

dissociation behavior. Ion signal intensities of the released and in an orthodox manner bound peptides increased proportional with increasing collision energy in sigmoidal shaped courses.

Quantitative analysis of gas phase complex dissociation reactions

Considering the above observations, ITEM-TWO analyses of the seven orthodox phospho-hexapeptide/anti-HpTGEKP antibody mixtures were investigated in duplicate measurement series except for phospho-hexapeptide HpTGERP (02). Mean charge states from ion series of the respective immune complexes (Table 2) were determined to be between 25.5+ (immune complex with phospho-hexapeptide 02) and 27.8+ (immune complexes with phospho-hexapeptides 06 and 09, respectively). The increase of product ion intensities, *i.e.* of complex-released phospho-hexapeptide ions and of freed antibody ions as a function of collision energy followed courses with Boltzmann characteristics (Table 2). Fitting goodness was around 0.99 in all cases. Apparent thermodynamic and apparent kinetic gas phase complex binding strengths were calculated for the seven orthodox binding peptides using the respective sigmoidal curve parameters. The course of the sigmoidal curve of the phospho-hexapeptide HpTGEKP (01)-anti-HpTGEKP antibody complex dissociation was set as standard because this phospho-hexapeptide contained the binding motif which was used to raise the monoclonal anti-HpTGEKP antibody. The high-mass ions were exposed to collision cell voltage differences up to 80 V which revealed that the group of orthodox binding phospho-hexapeptides could be divided into two subgroups.

The first subgroup of orthodox binding phospho-hexapeptides consists of immune complexes whose gas phase dissociation reactions followed similar courses to that of the standard immune complex (Figure 3A), comprising phospho-hexapeptides HpTGEKP (01), HpTGERP (02), HpSGERP (06), and HpTGEKL (07). As expected, the respective Arrhenius plots which provide information of the temperature dependencies of all four immune complex dissociation reactions revealed nearly overlapping lines and comparable $k_{m0g}^{\#}$ values at T_{amb} (Figure 3B, Table 3). The Gibbs-Helmholtz plot mirrored these similarities and afforded comparable $K_{D,m0g}^{\#}$ values at T_{amb} for all four

Table 2. Course characteristics of immune complex gas phase dissociations for orthodox binding phospho-hexapeptides and anti-HpTGEKP antibody.

Complex no. ^[a]	Phospho-hexapeptide sequence	Mean charge \pm std. dev. ^[b,c]	Initial amount [%] ^[b,c,d]	Final amount [%] ^[b,c,e]	ΔCV_{50} [V] ^[b,f]	Dx [V] ^[b]	Slope [%/V] ^[b]	$R^{2[b,c]}$
05	HpTGKPP	27.1 \pm 0.65	18.8	90.6	14.1	3.8	+4.7	0.987
10	HpTREKP	27.3 \pm 0.21	7.1	88.4	18.9	6.8	+3.0	0.989
07	HpTGEKL	26.7 \pm 0.18	24.7	76.9	21.4	11.7	+1.1	0.991
06	HpSGERP	27.8 \pm 0.04	41.3	78.4	22.9	10.3	+0.9	0.989
02	HpTGERP	25.5	6.5	71.1	25.5	11.9	+1.4	0.989
09	HpTEEKP	27.7 \pm 0.11	39.5	75.9	26.2	14.3	+0.6	0.990
01	HpTGEKP	27.1 \pm 0.09	17.5	74.2	27.2	11.3	+1.3	0.993

[a] Multiply charged and accelerated complex. [b] Averaged from two measurement series except for phospho-hexapeptide 02. [c] Unitless number. [d] Product amount at lowest applied ΔCV . [e] Product amount at highest applied ΔCV . [f] Entries are sorted by experimentally determined ΔCV_{50} values in ascending order.

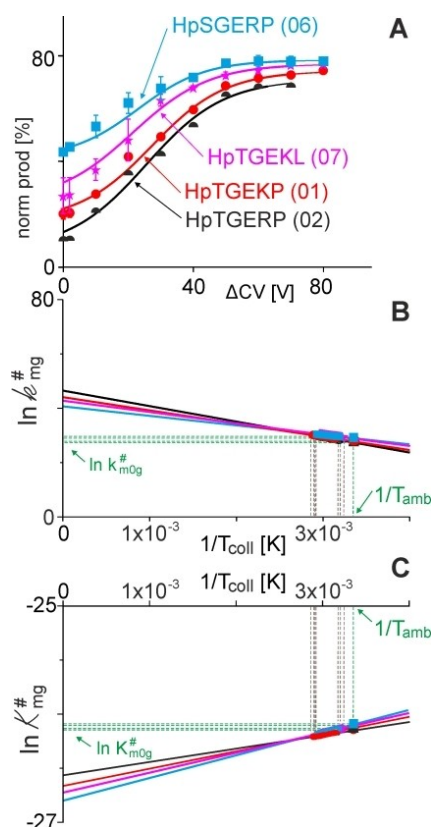


Figure 3. ITEM-TWO analysis of immune complex dissociations containing either phospho-hexapeptide HpTGEKP (01), HpTGERP (02), HpSGERP (06), or HpTGEKL (07). (A) Courses of normalized ion intensities of phospho-hexapeptide-anti-HpTGEKP antibody immune complex ions (norm (products)) are shown as a function of collision cell voltage differences (ΔCV). Each data point is the mean value of two independent determinations. Vertical bars indicate standard deviations. The sigmoidal shaped curves were fitted using a Boltzmann equation function. Curve parameters used for calculations are shown in Table 2. Phospho-hexapeptides are color-coded. (B) Arrhenius plot for the courses of phospho-hexapeptide-anti-HpTGEKP antibody immune complex dissociations in the gas phase. Line colors as in (A). At $1/T_{amb}$ the values for $\ln k_{m0g}^{\#}$ are taken. (C) Gibbs-Helmholtz plot for the courses of phospho-hexapeptide-anti-HpTGEKP antibody immune complex dissociations in the gas phase. Line colors as in (A). Values for $\ln K_{m0g}^{\#}$ are taken at $1/T_{amb}$. Calculated kinetic and thermodynamic values of gas phase dissociations of immune complexes are listed in Table 3. Each data point (thickened parts of the lines in (B) and (C)) has been obtained experimentally; lines have been linearly extrapolated.

immune complex dissociation reactions as well (Figure 3C, Table 3).

The second subgroup of orthodox binding phospho-hexapeptides contained immune complexes whose gas phase dissociation reactions deviated substantially from the course of the phospho-hexapeptide HpTGEKP (01) immune complex dissociation (Figure 4A). This subgroup comprises immune complexes with phospho-hexapeptides HpTGKKP (05), HpTEEKP (09), and HpTREKP (10), respectively. Consequently, the respective Arrhenius plots revealed quite different slopes of the lines which reflect the temperature dependences of the complex dissociation reactions (Figure 4B) when compared to that of the immune complex dissociation reaction of the immune complex with phospho-hexapeptide HpTGEKP (01). Differences in the slopes of the lines were also evident in the Gibbs-Helmholtz plots (Figure 4C), indicating different kinetic and thermodynamic properties of the respective immune complex dissociation reactions. Yet, the $k_{m0g}^{\#}$ values at T_{amb} and the $K_{D,m0g}^{\#}$ values at T_{amb} were all in the same range and rather similar for the dissociation reactions of all seven orthodox bound phospho-hexapeptide-anti-HpTGEKP antibody immune complexes (Table 3).

The $\Delta H_{m0g}^{\#}$ values of the reference phospho-hexapeptide HpTGEKP (01)-anti-HpTGEKP antibody immune complex and of the immune complexes which contained phospho-hexapeptides HpTGERP (02), HpSGERP (06), and HpTGEKL (07), *i.e.* those which showed comparable dissociation courses (*cf.* Figure 3A), were all between approx. -1.0 kJ/mol and -1.5 kJ/mol.

By contrast, when the complex dissociation followed a much shallower course than that of the reference immune complex (*cf.* Figure 4A), which was seen for the immune complex containing phospho-hexapeptide HpTEEKP (09), the $\Delta H_{m0g}^{\#}$ value was distinctively lower, approx. -2.0 kJ/mol (Table 3). On the contrary, when the course of complex dissociation was much steeper than that of the reference immune complex (*cf.* Figure 4A), which was seen for the immune complexes with either phospho-hexapeptide HpTGKKP (05) or the phospho-hexapeptide HpTREKP (10), the $\Delta H_{m0g}^{\#}$ values were much higher, approx. $+0.3$ kJ/mol and $+1.8$ kJ/mol, respectively (Table 3). When, $\Delta H_{m0g}^{\#}$ values are positive, heat is taken up from the environment during complex dissociation (endothermic reaction). On the opposite, when $\Delta H_{m0g}^{\#}$ values are negative, heat is emitted during complex

Table 3. Apparent kinetic and apparent thermodynamic values for gas phase dissociations of immune complexes consisting of orthodox binding phospho-hexapeptide-anti-HpTGEKP antibody.

Complex no. ^[a]	Phospho-hexapeptide sequence	$k_{m0g}^{\#}$ [1/s] ^[b]	$K_{D,m0g}^{\#}$ [-] ^[b,c]	$\Delta G_{m0g}^{\#}$ [kJ/mol] ^[b]	$\Delta H_{m0g}^{\#}$ [kJ/mol] ^[b]	$T_{amb} \Delta S_{m0g}^{\#}$ [kJ/mol] ^[b]
05	HpTGKKP	4.1×10^{11}	4.31×10^{-12}	+ 64.84	+ 1.81	-63.01
10	HpTREKP	4.5×10^{11}	4.32×10^{-12}	+ 64.83	+ 0.28	-64.54
07	HpTGEKL	2.3×10^{12}	4.58×10^{-12}	+ 64.69	-1.52	-66.20
06	HpSGERP	3.6×10^{12}	4.66×10^{-12}	+ 64.65	-1.75	-66.38
02	HpTGERP	7.5×10^{11}	4.40×10^{-12}	+ 64.79	-1.09	-65.86
09	HpTEEKP	4.0×10^{12}	4.67×10^{-12}	+ 64.64	-2.03	-66.65
01	HpTGEKP	1.1×10^{12}	4.47×10^{-12}	+ 64.75	-1.38	-66.11

[a] Neutral and resting complex; T_{amb} : 298 K; entries are sorted as in Table 2. [b] Derived from two measurement series except for phospho-hexapeptide 02. [c] Unitless number.

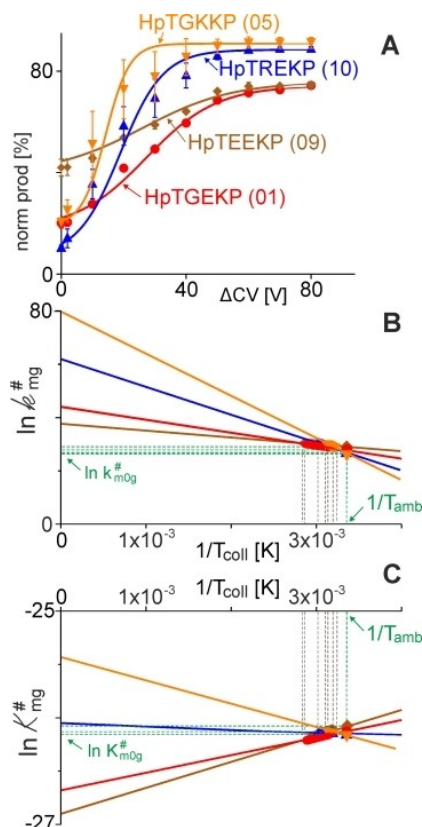


Figure 4. ITEM-TWO analysis of immune complex dissociations containing either phospho-hexapeptide HpTGEKP (01), HpTGKPK (05), HpTEEKP (09), or HpTREKP (10). (A) Courses of normalized ion intensities of phospho-hexapeptide-anti-HpTGEKP antibody immune complex ions (norm (products)) are shown as a function of collision cell voltage differences (ΔCV). Each data point is the mean value of two independent determinations. Vertical bars indicate standard deviations. The sigmoidal shaped curves were fitted using a Boltzmann equation function. Curve parameters used for calculations are shown in Table 2. Phospho-hexapeptides are color-coded. (B) Arrhenius plot for the courses of phospho-hexapeptide-anti-HpTGEKP antibody immune complex dissociations in the gas phase. Line colors as in (A). At $1/T_{amb}$ the values for $\ln k_{m0g}^{\#}$ are taken. (C) Gibbs-Helmholtz plot for the courses of phospho-hexapeptide-anti-HpTGEKP antibody immune complex dissociations in the gas phase. Line colors as in (A). Values for $\ln K_{m0g}^{\#}$ are taken at $1/T_{amb}$. Calculated kinetic and thermodynamic values of gas phase dissociations of immune complexes are listed in Table 3. Each data point (thickened parts of the lines in (B) and (C)) has been obtained experimentally; lines have been linearly extrapolated.

dissociation into the environment (exothermic reaction). Because $\Delta G_{m0g}^{\#}$ values of complex dissociation reactions are positive, the reaction is endergonic, hence, not spontaneous which means that the reverse reaction, complex formation, is exergonic and spontaneous.

To show that unorthodox binding indeed involved binding of the respective peptide with the paratope, we conducted a competition experiment in which a ternary mixture had been generated. Peptide 02 “HpTGERP” (considered an orthodox binder) and peptide 08 “HpTGEKS” (considered an unorthodox binder) were mixed with the anti-HpTGEKP antibody in 3:3:1 molar ratios. Under ITEM-TWO conditions only peptide 02 “HpTGERP” was detected in the respective mass spectra at elevated collision cell voltage differences and after blocking of

transmission of unbound peptides. We interpret this result as proof that both peptides had competed for binding to the paratope but only peptide 02 (with orthodox binding fashion) succeeded and exclusively occupied the paratope pocket (Supporting Information Figure S33).

Dissociation enthalpy ranking and immune complex competitive replacement assay

As peptide-antibody interactions depend on developing specific intermolecular forces between the two partners, it might be assumed that the determined gas phase immune complex stabilities might correlate with physicochemical properties, such as pI values of the phospho-hexapeptides. However, a summarizing peptide feature, such as pI (cf. Table 1), correlates with a “molecular recognition code” where distinct surface charge/polarity patterns are recognized by a binding antibody only with short peptides; hexa-peptides are short enough for correlation. A summarizing feature becomes meaningless with larger peptides and proteins.

At last, an antibody-phospho-peptide immune complex competitive replacement assay was performed to test whether the differences in the phospho-hexapeptides' binding properties towards the anti-HpTGEKP antibody which were determined by ITEM-TWO in the gas phase reflected the phospho-hexapeptides' in-solution binding properties to some extent. Western blot analysis showed in fact that the antibody's binding capacity towards its antigens which were displayed as PVDF membrane surface-bound proteins from cell extracts was affected by pre-incubation of the anti-HpTGEKP antibody with a phospho-hexapeptide. The three orthodox binding phospho-hexapeptides HpTGEKP (01), HpTEEKP (09), and HpTREKP (10) were able to substantially reduce or even prevent antibody decoration of zinc finger proteins (Figure 5) whereas the

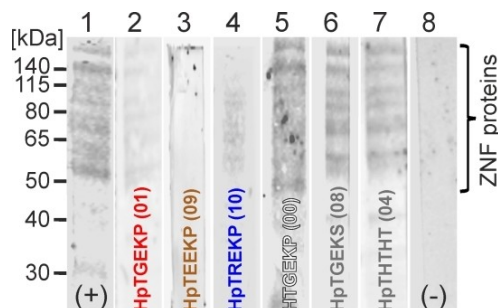


Figure 5. In-vitro competitive replacement assays. Protein extracts from C631 cells with exposure to okadaic acid as phosphatase inhibitor presented the antigens. The primary anti-HpTGEKP antibody had been incubated with the respective phospho-hexapeptide prior to decoration of proteins. IRDye 800 CW conjugated anti-mouse antibody from goat was used as secondary antibody. Lane 1: no peptide incubation (positive control, (+)). Lane 2: Phospho-hexapeptide HpTGEKP (01). Lane 3: Phospho-hexapeptide HpTEEKP (09). Lane 4: Phospho-hexapeptide HpTREKP (10). Lane 5: Hexapeptide HTGEKP (00). Lane 6: Phospho-hexapeptide HpTGEKS (08). Lane 7: Phospho-hexapeptide HpTHHT (04). Lane 8: no primary anti-HpTGEKP antibody (negative control, (-)). Blot images have been cropped approx. above 200 kDa and approx. below 25 kDa, respectively.

unorthodox binding phospho-hexapeptides HpTHTHT (04) and HpTGEKS (08) did not. In this respect the unorthodox binding phospho-hexapeptides behaved like the non-binding hexapeptide HTGEKP (00).

Clearly, strong gas phase binding corresponds with efficient paratope blocking in solution. Thus, the ITEM-TWO results stand in agreement with data from in-solution immuno-assays.

Discussion

Protein phosphorylation has been addressed as one of the most important post-translational modifications which caused switching from one protein activity state to another or from a protein bound state to an unbound state;^[19] the latter is of importance for zinc finger proteins which have to bind to DNA and to other proteins to exert their biological functions, such as regulation of gene expression.^[10]

When performing molecular dynamics calculations and analyzing the plot of RMSD vs time (Figure 6) it becomes evident that for the un-phosphorylated linker there is a well-defined and highly populated basin at low RMSD ($< 19 \text{ \AA}$) which corresponds to zinc finger proteins with a ZF2 domain located close to the DNA bound conformation (ON state) and a less

populated basin at high RMSD ($> 25 \text{ \AA}$) which indicates an equivalent to the DNA remote location of a ZF2 domain (OFF state). By contrast, when the linker is phosphorylated, the switching dynamics between the two conformations, ON state/OFF state, increases dramatically. Similar frequency increases between two states, *i.e.* protein conformation, have been published for other protein systems,^[20] indicating that changing molecular dynamics upon phosphorylation was a common mechanism which nature applies for regulatory purposes, *e.g.* to control cellular processes, such as maturation and proliferation.^[21] With respect to zinc finger protein analyses one has to keep in mind that when working with whole cell extracts the highly specific anti-HpTGEKP antibody decorates a distinct pool of predominantly non-DNA-bound zinc finger proteins because it recognizes exclusively phosphorylated linkers which carry the anti-HpTGEKP antibody-recognition motif.

Molecular recognition code principles, termed epitope-antibody recognition mode, had been elucidated from studies on IVlg which allowed categorizing antibody paratopes according to their physicochemical properties like polarity and hydrophobicity.^[22] We suggest using the term orthodox epitope-paratope interactions for such noncovalent bindings which rely on forces which unfold between single atoms placed on molecular partial surfaces with the right physico-chemical properties on precisely matching positions on molecular surfaces located opposite to each other^[14] either by nature or by design. With ITEM-TWO the distinction between orthodox and unorthodox binding can be made with consuming very little material. Of note, in the here described studies all in-solution conditions had been kept constant, so the experimentally determined complex dissociation differences are a result of the amino acid sequence differences in the studied phospho-hexapeptides, which stands in agreement with previous investigations on the ITEM method's scope and limitations.^[15a,23]

Other approaches for determining molecular diversities of antibodies applied "combinatorial alanine scanning"^[24] or in-silico mutagenesis methods^[25] in combination with phage display to identify strategic residues at the interface of antigen-antibody interactions and require significant mutagenesis efforts^[26] whereas in our approach chemical peptide synthesis routines were exploited for fine mapping of epitopes. Scope and limitation of epitope fine mapping methods have been reviewed^[27] and emphasized the still existing bottle neck in methods for determining the contributions of single amino acid residues for molecular recognition and binding affinity.

Conclusion

Our ITEM-TWO analyses of the anti-HpTGEKP antibody reveal a bipolar motif for binding of phospho-hexapeptides in an orthodox manner: an N-terminally located negative charge, the phosphorylated threoninyl residue (pT) on the phospho-hexapeptides is accompanied by a C-terminally located positive charge, the dipeptidyl residue (KP, RP, or KL). Unorthodox fashion of binding is found with phospho-hexapeptides which in addition to the phosphorylated threoninyl residue (pT)

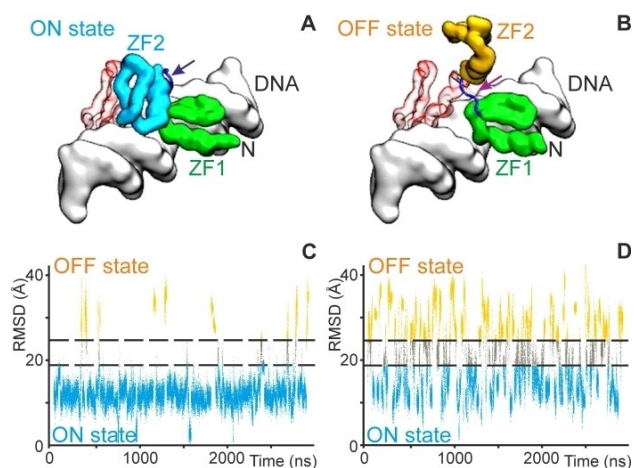


Figure 6. Snapshots (A, B) of configurations of two zinc finger domains attached to the major groove of the DNA double helix (white) and plot of second zinc finger (ZF2) movements (C, D) as it is exploring the phase space over physical time (ns) of simulation. (A, B) The first zinc finger domain (ZF1; green) is fixed and superimposed on the first zinc finger domain of the Zif268/DNA X-ray structure (1aay.pdb). The red transparent zinc finger structure image indicates the position of the second zinc finger domain of the Zif268/DNA X-ray structure. The letter "N" marks the position of the N-terminus. (A) The linker hexapeptide HTGEKP is shown as a dark blue line (dark blue arrow) which connects the first (ZF1; green) with the second (ZF2; cyan) zinc finger domain. (B) The linker phospho-hexapeptide HpTGEKP (dark red arrow) is shown as a dark blue line which connects the first (ZF1; green) with the second (ZF2; yellow) zinc finger domain. Simulation time points are 925 ns, each. ON state: ZF2 is located in a position near the major groove. OFF state: ZF2 is located in a position away from the major groove. (C, D) The RMSD (root mean square deviation; \AA) is used as a measure of location of ZF2 near to the major groove (ON state) or away from the major groove (OFF state). Borders between states are defined at 19 \AA (lower horizontal dashed line: ON state is below) and at 25 \AA (upper horizontal dashed line: OFF state is above).

provide a C-terminally located hydroxyl-containing amino acid (T, S) or instead of the N-terminal phosphorylated threoninyl residue (pT) possess a phosphorylated serinyl residue, or when they display non-canonical amino acid sequences. Our data further confirm that in complete absence of phosphorylation at position 2, the hexapeptide HTGEKP (00) does not bind to the anti-HpTGEKP antibody.

Experimental Section

Cell cultivation and protein extract generation: Adherently growing HAP1 cells (C631) were cultivated^[28] and harvested^[29] as described. For details see Supporting Information.

SDS-PAGE and Western blot analysis: SDS-PAGE analysis^[30] of protein extracts and Western blotting^[31] of proteins was done as previously described^[32] using standard protein staining^[33] and fluorescence imaging^[34] methods. For details see Supporting Information.

Nanospray offline mass spectrometric ITEM-TWO analyses: Nano-ESI offline mass spectrometric measurements and ITEM-TWO analyses^[23,35] were performed as previously described. For details see Supporting Information. The mass spectrometry data were forwarded to the ProteomeXchange Consortium and deposited in the PRIDE^[36] partner repository with the dataset identifier PXD031150.

Antibody-phospho-peptide immune complex competitive replacement assay: For the antibody-phospho-peptide immune complex competitive replacement assay a modified Western blot procedure was applied as is detailed in the Supporting Information.

Molecular dynamics and in-silico analysis: The molecular dynamics of Zif268 was simulated using the 1AAY.pdb structure file^[37] from the Protein Data Bank.^[38] The Amber99sb-ILDN force field^[39] and TIP3P model^[40] were used for modelling proteins, ions, and water, respectively. Simulations were performed in the NPT ensemble (constant number of particles, pressure and temperature) using the GROMACS 2019 software.^[41] Molecular representations were generated using Visual Molecular Dynamics.^[42] For details see Supporting Information.

Acknowledgements

Mr. M. Kreutzer is acknowledged for his help with the bioinformatics platform and upload of raw data to PRIDE. This research was funded by in-house sources of the Proteome Center Rostock, the IndyMED GmbH, and the University of Medicine and Pharmacy of Iasi. Open Access funding enabled and organized by Projekt DEAL.

Conflict of Interest

The authors declare no conflict of interest.

Data Availability Statement

The mass spectrometry data were forwarded to the ProteomeXchange Consortium and deposited in the PRIDE^[36] partner repository with the dataset identifier PXD031150.

Keywords: antibodies · binding strength · dissociation constants · ESI-MS · immune complexes · ITEM-TWO · mass spectrometry

- [1] S. A. Lambert, A. Jolma, L. F. Campitelli, P. K. Das, Y. Yin, M. Albu, X. Chen, J. Taipale, T. R. Hughes, M. T. Weirauch, *Cell* **2018**, *172*, 650–665.
- [2] J. H. Laity, B. M. Lee, P. E. Wright, *Curr. Opin. Struct. Biol.* **2001**, *11*, 39–46.
- [3] S. Bu, Y. Lv, Y. Liu, S. Qiao, H. Wang, *Front. Neurol. Neurosci.* **2021**, *15*, 760567.
- [4] a) X. Li, M. Han, H. Zhang, F. Liu, Y. Pan, J. Zhu, Z. Liao, X. Chen, B. Zhang, *Biomark. Res.* **2022**, *10*, 2; b) D. Munro, D. Ghersi, M. Singh, *PLoS Comput. Biol.* **2018**, *14*, e1006290.
- [5] M. A. Hossain, J. J. Barrow, Y. Shen, M. I. Haq, J. Bungert, *J. Cell. Biochem.* **2015**, *116*, 2435–2444.
- [6] M. S. Bhakta, D. J. Segal, *Meth. Mol. Biol.* **2010**, *649*, 3–30.
- [7] S. Dovati, T. Ronni, D. Russell, R. Ferrini, B. S. Cobb, S. T. Smale, *Genes Dev.* **2002**, *16*, 2985–2990.
- [8] a) M. Y. Hamed, R. Siam, R. Zaid, *J. Comput.-Aided Mol. Des.* **2021**, *35*, 973–986; b) L. Luo, S. Ando, Y. Sakamoto, T. Suzuki, H. Takahashi, N. Ishibashi, S. Kojima, D. Kurihara, T. Higashiyama, K. T. Yamamoto, *Plant J.* **2020**, *101*, 1118–1134.
- [9] a) D. Jantz, J. M. Berg, *Proc. Nat. Acad. Sci. USA* **2004**, *101*, 7589–7593; b) R. Rizkallah, K. E. Alexander, M. M. Hurt, *Cell Cycle* **2011**, *10*, 3327–3336.
- [10] T. Sekiya, K. Murano, K. Kato, A. Kawaguchi, K. Nagata, *FEBS Open Bio.* **2017**, *7*, 397–404.
- [11] B. Elbaz, J. D. Aaker, S. Isaac, A. Kolarzyk, P. Brugarolas, A. Eden, B. Popko, *Cell Rep.* **2018**, *23*, 2254–2263.
- [12] a) J. Jen, Y. C. Wang, *J. Biomed. Sci.* **2016**, *23*, 53; b) K. Suzuki, K. Sako, K. Akiyama, M. Isoda, C. Senoo, N. Nakajo, N. Sagata, *Sci. Rep.* **2015**, *5*, 7929.
- [13] C. B. Saper, *J. Histochem. Cytochem.* **2009**, *57*, 1–5.
- [14] K. F.-M. Opuni, M. Al-Majdoub, Y. Yefremova, R. F. El-Kased, C. Koy, M. O. Glocker, *Mass Spectrom. Rev.* **2018**, *37*, 229–241.
- [15] a) Y. Yefremova, K. F.-M. Opuni, B. D. Danquah, H.-J. Thiesen, M. O. Glocker, *J. Am. Soc. Mass Spectrom.* **2017**, *28*, 1612–1622; b) Y. Yefremova, B. D. Danquah, K. F.-M. Opuni, C. Röwer, C. Koy, M. O. Glocker, *J. Proteom.* **2019**, *212*, 103572; c) B. D. Danquah, C. Röwer, K. F.-M. Opuni, R. F. El-Kased, D. Frommholz, H. Illges, C. Koy, M. O. Glocker, *Mol. Cell. Proteomics* **2019**, *18*, 1543–1555.
- [16] Y. Yefremova, B. D. Danquah, K. F.-M. Opuni, R. F. El-Kased, C. Koy, M. O. Glocker, *Eur. J. Mass Spectrom.* **2017**, *23*, 445–459.
- [17] B. Skoog, A. Wichman, *Trends Anal. Chem.* **1986**, *5*, 82–83.
- [18] Y. Xie, Y. Jiang, D. Ben-Amotz, *Anal. Biochem.* **2005**, *343*, 223–230.
- [19] H. Nishi, A. Shaytan, A. R. Panchenko, *Front. Genet.* **2014**, *5*, 270.
- [20] W. Han, J. Zhu, S. Wang, D. Xu, *J. Phys. Chem. B* **2017**, *121*, 3565–3573.
- [21] D. J. Lew, S. Kornbluth, *Curr. Opin. Cell Biol.* **1996**, *8*, 795–804.
- [22] M. Luštrek, P. Lorenz, M. Kreutzer, Z. Qian, F. Steinbeck, D. Wu, N. Born, B. Ziemer, M. Hecker, M. Blank, Y. Shoenfeld, Z. Cao, M. O. Glocker, Y. Li, G. Füllen, H.-J. Thiesen, *PLoS One* **2013**, *8*, e78605.
- [23] a) B. D. Danquah, K. F.-M. Opuni, C. Roewer, C. Koy, M. O. Glocker, *Molecules* **2020**, *25*, 4776; b) C. Koy, K. F.-M. Opuni, B. D. Danquah, A. Neamtu, M. O. Glocker, *Int. J. Mol. Sci.* **2021**, *22*, 10183.
- [24] a) G. Robin, Y. Sato, D. Desplancq, N. Rochel, E. Weiss, P. Martineau, *J. Mol. Biol.* **2014**, *426*, 3729–3743; b) G. A. Weiss, C. K. Watanabe, A. Zhong, A. Goddard, S. S. Sidhu, *Proc. Nat. Acad. Sci. USA* **2000**, *97*, 8950–8954.
- [25] L. Xin, H. Yu, Q. Hong, X. Bi, X. Zhang, Z. Zhang, Z. Kong, Q. Zheng, Y. Gu, Q. Zhao, J. Zhang, S. Li, N. Xia, *Interdisc. Sciences: Comput. Life Sci.* **2018**, *10*, 438–448.
- [26] D. Bannister, B. Popovic, S. Sridharan, F. Giannotta, P. Filée, N. Yilmaz, R. Minter, *Protein Eng.* **2010**, *24*, 351–360.
- [27] W. M. Abbott, M. M. Damschroder, D. C. Lowe, *Immunology* **2014**, *142*, 526–535.

- [28] N. Born, H.-J. Thiesen, P. Lorenz, *PLoS One* **2014**, *9*, e87609.
- [29] R. Bajpai, J. Lesperance, M. Kim, A. V. Tersikh, *Mol. Reprod. Dev.* **2008**, *75*, 818–827.
- [30] P. Lorenz, D. Koczan, H.-J. Thiesen, *Biol. Chem.* **2001**, *382*, 637–644.
- [31] K. F.-M. Opuni, S. Solomon, F. Metzger, D. Frommholz, C. Koy, C. Röwer, M. O. Glocker, H. Illges, P. Anderson, *J. Proteom. Bioinform.* **2017**, *10*, 60–72.
- [32] C. Röwer, J. P. Vissers, C. Koy, M. Kipping, M. Hecker, T. Reimer, B. Gerber, H.-J. Thiesen, M. O. Glocker, *Anal. Bioanal. Chem.* **2009**, *395*, 2443–2456.
- [33] D.-H. Kang, Y.-S. Gho, M.-K. Suh, C.-H. Kang, *Bull. Korean Chem. Soc.* **2002**, *23*, 1511–1512.
- [34] M. Al Chiblak, F. Steinbeck, H.-J. Thiesen, P. Lorenz, *BMC Mol. Cell Biol.* **2019**, *20*, 1–23.
- [35] K. F.-M. Opuni, C. Koy, M. Russ, M. Reepmeyer, B. D. Danquah, M. Weresow, A. Alef, P. Lorenz, H.-J. Thiesen, M. O. Glocker, *J. Biol. Chem.* **2020**, *295*, 14987–14997.
- [36] Y. Perez-Riverol, A. Csordas, J. Bai, M. Bernal-Llinares, S. Hewapathirana, D. J. Kundu, A. Inuganti, J. Griss, G. Mayer, M. Eisenacher, *Nucleic Acids Res.* **2019**, *47*, D442–D450.
- [37] M. Elrod-Erickson, M. A. Rould, L. Nekludova, C. O. Pabo, *Structure* **1996**, *4*, 1171–1180.
- [38] H. M. Berman, J. Westbrook, Z. Feng, G. Gilliland, T. N. Bhat, H. Weissig, I. N. Shindyalov, P. E. Bourne, *Nucleic Acids Res.* **2000**, *28*, 235–242.
- [39] K. Lindorff-Larsen, S. Piana, K. Palmo, P. Maragakis, J. L. Klepeis, R. O. Dror, D. E. Shaw, *Proteins Struct. Funct. Bioinf.* **2010**, *78*, 1950–1958.
- [40] P. Mark, L. Nilsson, *J. Phys. Chem. A* **2001**, *105*, 9954–9960.
- [41] M. J. Abraham, T. Murtola, R. Schulz, S. Páll, J. C. Smith, B. Hess, E. Lindahl, *SoftwareX* **2015**, *1*, 19–25.
- [42] W. Humphrey, A. Dalke, K. Schulten, *J. Mol. Graphics* **1996**, *14*, 33–38.

Manuscript received: July 12, 2022

Revised manuscript received: August 3, 2022

Accepted manuscript online: August 11, 2022

Version of record online: September 12, 2022